Biomass, thermal inertia, and radiative freeze occurrence in leafless forests

Brian E. Potter and John C. Zasada

Abstract: Using field measurements of air temperature, wind, and relative humidity from a clear-cut site and two wooded sites in northern Wisconsin, we used a radiative transfer model to simulate temperatures on seven calm, clear nights similar to those on which freezes typically occur. Each night was simulated twice for the wooded sites. One simulation ignored the presence of vegetation, the other approximated the vegetation's heat storage capacity and its influence on air temperatures. The simulations including biomass heat storage showed smaller mean absolute temperature errors and decreased magnitude of systematic model error when compared with the simulations ignoring vegetation. The results suggest that the thermal inertia of forest biomass may play a significant role in controlling forest temperatures on calm, clear nights and, hence, in controlling freeze occurrence.

Résumé : À l'aide de mesures de la température de l'air, du vent et de l'humidité relative prises sur le terrain dans un site coupé à blanc et deux sites boisés dans le nord du Wisconsin, nous avons utilisé un modèle de transfert radiatif pour simuler la température lors de sept nuits claires et calmes semblables à celles où se produisent typiquement les gels. Chaque nuit a été simulée deux fois pour les sites boisés. Une simulation faisait abstraction de la présence de végétation et l'autre tenait compte de la capacité d'emmagasinage de la chaleur par la végétation et de son influence sur la température de l'air. Les simulations qui comportaient le stockage de chaleur par la biomasse montraient de plus faibles erreurs moyennes absolues de température et diminuaient l'importance de l'erreur systématique du modèle comparativement aux simulations qui ignoraient la végétation. Les résultats suggèrent que l'inertie thermale de la biomasse forestière pourrait jouer un rôle important dans le contrôle de la température de la forêt par nuits claires et calmes et, par conséquent, dans le contrôle des épisodes de gel.

[Traduit par la Rédaction]

Introduction

Freezes that occur in late spring can have a significant impact on vegetation. They can kill new seedlings and new growth on established trees, slowing the growth of these trees and perhaps allowing other species to become established. In economic terms, the change in species may be undesirable.

Meteorologists recognize two general mechanisms that produce such freezes: advection and radiation. Advective freezes result from movement of cold air into an area, can occur at any time of the day, and rarely produce hoarfrost. The scale of such air movement can be anything from local, such as a drainage flow from an adjacent hillside, to synoptic, as in passage of a cold front. They show little vertical temperature variation, depend weakly on ground conditions, and usually result in air temperatures less than the temperature of the soil surface. Radiative freezes begin at the ground and spread upward into the air over time. They occur only at night under the calmest wind conditions, and often result in hoarfrost. During a radiative freeze event, the ground surface temperature will always be less than the temperature of the air above it, and air temperatures will usually increase with height in the lowest 50–100 m. Figure 1*a* shows temperatures at the soil surface and air temperatures at 2.5 and 10 m during a typical advective freeze; Fig. 1*b* shows temperatures for a radiative freeze event. In both cases, temperatures at 0.25 m fell below 0°C.

Because an advective freeze is not linked to the local ground conditions, it chills the vegetation in forests and fields comparably. The freezing air moves into or across trees, rivers, and open fields regardless of the state of vegetation. If an advective freeze is going to kill vegetation, it will probably do so no matter what the density of vegetation in the location.

Radiative freezes are quite different in this respect. Anything that keeps the ground from cooling below freezing can prevent a radiative freeze. Possible reasons the ground might not cool below freezing include moist soil, some sort of cover that radiates energy back to the ground surface, or physical structures such as trees, large rock outcrops, or buildings atop the soil.

Where radiative freezing may occur, the thermal protection of forest vegetation can be important. The energy radiated towards the ground by overstory foliage, almost always greater than the energy the ground would receive from a clear or even cloudy sky, reduces net energy loss at the surface and reduces nocturnal cooling. In addition, the mass of the trees has a greater heat capacity than an equal volume of air, so that the total thermal inertia of the subcanopy layer

Received July 9, 1998. Accepted December 10, 1998.

B.E. Potter.[1] USDA Forest Service, North Central Research Station, Room 220, 1407 South Harrison Road, East Lansing, MI 48823, U.S.A. e-mail: potterb@pilot.msu.edu
J.C. Zasada. Forestry Sciences Laboratory, 1831 Highway 169 East, Grand Rapids, MN 55744-3399, U.S.A. e-mail: jzasada/nc_rh@fs.fed.us

[1]Author to whom all correspondence should be addressed.

Fig. 1. Nighttime temperatures at the soil surface (solid line) and at 2.5 m (long-dash broken line) and 10 m (short-dash broken line) aboveground (*a*) during a typical advective freeze and (*b*) during a typical radiative freeze.

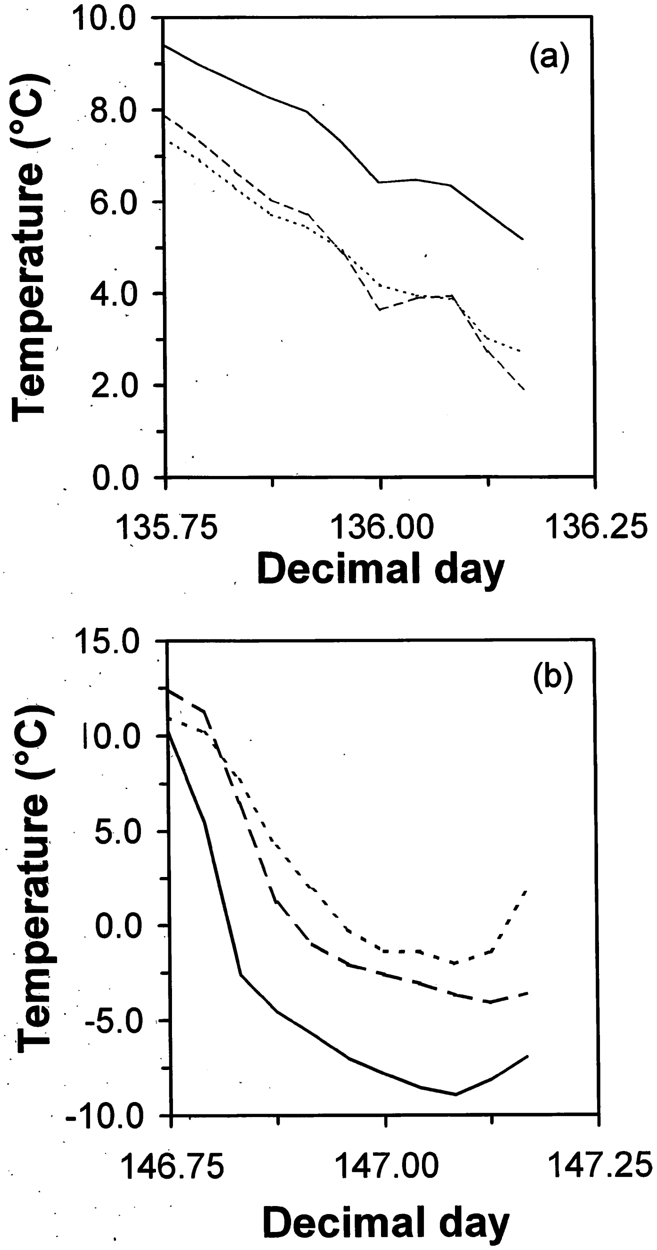

Fig. 2. Field study plot configuration and location.

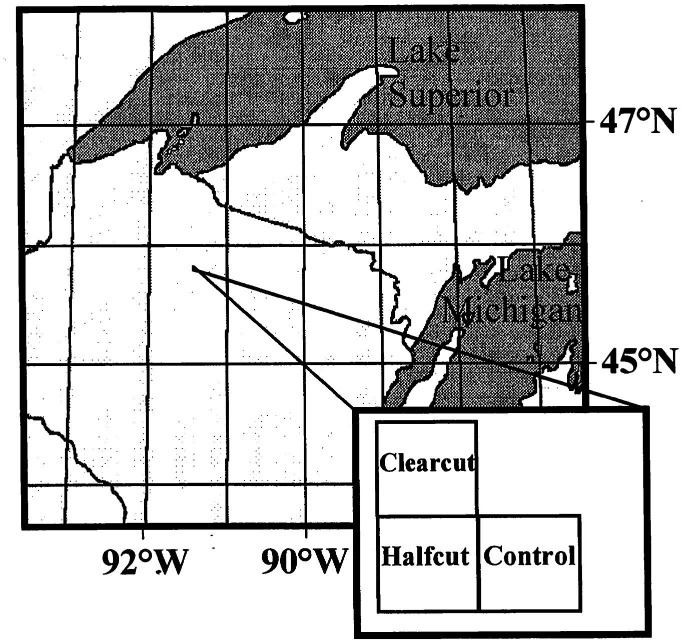

increases because of the presence of trees. The role of thermal inertia may be particularly important during middle and late spring, when there is no canopy foliage yet, and radiative freezes could kill emerging growth near the ground.

Many authors (e.g., Kittredge 1948; Geiger 1965; Aussenac 1970; Ringer and Stearns 1972; Anderson and Brower 1996) have mentioned the association between the degree of cover provided by a forest canopy and the amount by which temperatures beneath that canopy are altered. A few authors, such as Baumgartner (1956), Munn (1966), Arya (1988), and Meesters and Vugts (1996) have acknowledged the influence of biomass heat storage in controlling forest temperatures.

Baumgartner (1956) noted that the biomass on his study site was the equivalent of a layer 1.89 cm deep over the entire forest area. The actual vegetation height was 5.6 m. Using a density for wood of 600 $kg \cdot m^{-3}$ and a specific heat of 2×10^3 $J \cdot kg^{-1} \cdot K^{-1}$ based on TenWolde et al. (1988), this biomass has a heat capacity of 2.3×10^4 $J \cdot K^{-1} \cdot m^{-2}$. The air in a layer 5.6 m deep, in comparison, has a heat capacity of roughly 6.2×10^3 $J \cdot K^{-1} \cdot m^{-2}$. Here, biomass accounts for 80% of the total aboveground heat capacity.

Through our literature search, we did not locate any attempt to demonstrate the magnitude of the impact biomass heat storage can have on nocturnal temperatures in a leafless forest. In this study, we examine the role of biomass thermal inertia in the evolution of nighttime temperatures in a leafless forest. We do this by applying a detailed infrared radiative transfer model (IRTM) to observations of nighttime temperatures in three sites with different vegetation densities.

Methods

Data

In 1988, we began a field experiment comprising four, 8-ha plots on the Chequamegon National Forest, near Park Falls, Wis. One plot was clearcut, another left uncut, a third had 25% of the overstory removed, and the fourth had half of the overstory removed. All sites have since been allowed to develop naturally, such that the clearcut is now covered with young aspen and some oak. The wooded sites have not changed as dramatically. The plots are on level to gently sloping terrain, with moderately well-drained sandy loam soil, and a canopy height of roughly 20 m. Tree species that dominate the wooded sites include white ash (*Fraxinus americana* L.), sugar maple (*Acer saccharum* Marsh.), basswood (*Tilia americana* L.), and red oak (*Quercus rubra* L.). Figure 2 shows the configuration of the four plots, and Table 1 summarizes the sites and their basal areas. Teclaw and Isebrands (1993) describe further details of the study site.

In 1994, meteorological instruments were installed to record hourly air temperatures, humidities, and wind speeds in the

Table 1. Basal areas for study sites at Willow Springs, Wis.

	Clearcut	50% crown	75% crown	100% crown
BA ($m^2 \cdot ha^{-1}$)	0.0	17.0	20.7	32.4

clearcut, half-cut, and uncut sites. (Henceforth, we will refer to the latter two sites collectively as the forest sites.) Thermistors and thermocouples measure temperature at 0.25, 0.5, 1.0, 2.5, and 10 m; relative humidity and horizontal wind speed are measured at 2.5 and 10 m. Twelve plate gill radiation shields house the thermistors. The thermocouples are 0.51-mm copper–constantan thermocouples, shielded with horizontal plates as described in Percy et al. (1989). These measurements have taken place continuously from January 1, 1994, to the present with few gaps in the data. The total instrumental error for the thermocouples is about 1.0 K, while the relative humidity measurement error is between 2% and 3% relative humidity. The wind speed measurements have a lower threshold of 0.2 $m \cdot s^{-1}$, and their error is approximately 2% of the measurement value (about 0.05 $m \cdot s^{-1}$ for the conditions in this study.)

From the complete set of 1994 and 1995 data for these sites, we selected nocturnal time periods when the conditions reflected calm spring nights. These nights must have little or no wind, no snow cover, no precipitation, and little or no cloud cover. Since the intent of this study was to examine biomass heat storage and nocturnal temperature evolution, it was not essential that temperature drop below freezing on a given night; any night on which radiative cooling was the dominant process will suffice for this purpose. We considered only the time period between sunset and sunrise for any given night.

The first step was selection of nights with little or no wind. We examined winds measured at 10 m in the clearcut site, and eliminated any night where the wind exceeded 2.5 $m \cdot s^{-1}$ during the night or where five or more hourly wind measurements exceeded 1.0 $m \cdot s^{-1}$.

On some nights, there were indications of significant nonradiative processes even though winds were calm. One such indicator was temperature rising part way through the night, well before sunrise. Another indicator of nonradiative processes was the equalization of temperatures at all heights. As mentioned previously, when radiation dominates temperatures are coldest near the ground and warmer aloft. Several nights began with this type of profile, but wind increased later and conditions changed abruptly to produce almost equal temperatures from 0.25 to 10 m. Only the portion of each night when temperatures were declining over time, and increasing with height, was retained for this study. If temperature at one or more heights increased for only 1 h, then decreased again for the remainder of the period, we retained the night.

We next examined National Weather Service surface weather observations from Rhinelander, Wis. (These are available from the National Climatic Data Center over the World Wide Web at http://www.ncdc.noaa.gov.) For those nights that passed the wind test, we checked cloud cover and precipitation and eliminated any night with reported precipitation. We required cloud cover to be no more than 25% below 7000 ft (1 ft = 0.305 m).

We retrieved radiosonde data for International Falls, Min. (IF), and Green Bay, Wis. (GB), for the remaining nights. Radiosonde data provide information on air temperature, pressure, wind, and relative humidity at various heights between the earth's surface and some height between 20 and 30 km. These measurements are made at 00:00 and 12:00 UTC, and past measurements are available from the National Climatic Data Center. Using radiosonde data from 00:00 UTC (which corresponds to 18:00 CST or 19:00 CDT), we plotted vertical profiles of relative humidity for the two locations mentioned. In such profiles, probable cloud layers are conspicuous as distinct layers of relative humidity exceeding 80%. If radiosonde data for GB or IF showed cloud, the day in question was dropped from the sample set.

Table 2. Nights retained for use in model simulations, showing calendar day, month and day, start and end times, and duration for each simulation.

Year and calendar day	Month and day	Period simulated (LST)	Duration (h)
1994			
100	April 10	18:00–01:00	7
152	June 1	19:00–04:00	9
304	October 31	17:00–05:00	12
313	November 9	17:00–24:00	7
1995			
103	April 13	19:00–05:00	10
125	May 5	20:00–04:00	8
137	May 17	20:00–04:00	8

The last two requirements for a night to be retained were that there be no indication in the data of snow being present and that the trees not be fully leafed out. We assessed the first condition by noting the temperatures at 0.25, 0.5, and 1.0 m. When snow was present, 0.25 m temperatures remained very steady over the night, while temperatures at the upper two levels dropped significantly.

We based our determination of whether the trees had significant amounts of foliage on daily average relative humidity differences between the half-cut site and the clear-cut site. When foliage is absent, these differences are much smaller than when foliage is present, as shown in Fig. 3. As an approximation, we kept only those nights prior to calendar day 153 or following day 265. Only one of the candidate days was near these limits, and that was day 152 from 1994.

When we had applied all of these tests, seven nights remained. Table 2 lists the nights and the time period used for this study for each night.

Model

An IRTM is a one-dimensional model that partitions the atmosphere into horizontally uniform layers, each represented by an average temperature, pressure, and moisture content. These properties determine the infrared emissivity of the layers. The emissivities, in conjunction with radiative transfer equations, subsequently determine the radiative flux divergence for that layer. Figure 4 shows schematically the model configuration for this study.

We used the IRTM of Liou et al. (1984). It calculates absorption by the H_2O rotation band at 15 mm, H_2O continuum at 10 mm, H_2O vibration–rotation at 6.3 mm, and CO_2 at 15 mm, and it adjusts for overlap between the H_2O rotation and CO_2 bands. The original model included absorption by ozone, but we omitted this. We added one microphysical process to the model, that being condensation or evaporation of water droplets to form fog. We assumed any such phase change would maintain thermodynamic equilibrium. Water droplet absorption and emission of infrared radiation follow the model of Stephens (1978).

Liou and Ou (1983) describe the parameterized emissivities used in the Liou et al. model. They developed the equations for water-vapor path lengths between 10^{-6} and 100 $kg \cdot m^{-2}$ and, for carbon dioxide, between 10^{-6} and 2.0 $kg \cdot m^{-2}$. The water vapor and carbon dioxide path lengths in the present study range from roughly 3×10^{-3} to 0.2 $kg \cdot m^{-2}$ and 1.8×10^{-4} to 0.01 $kg \cdot m^{-2}$, respectively, and are well within the intended range of values.

Fig. 3. Difference in average daily relative humidity (DRH) between half-cut and clear-cut sites. The broken line shows daily values, and the heavy solid line indicates a 7-day running average of the daily values.

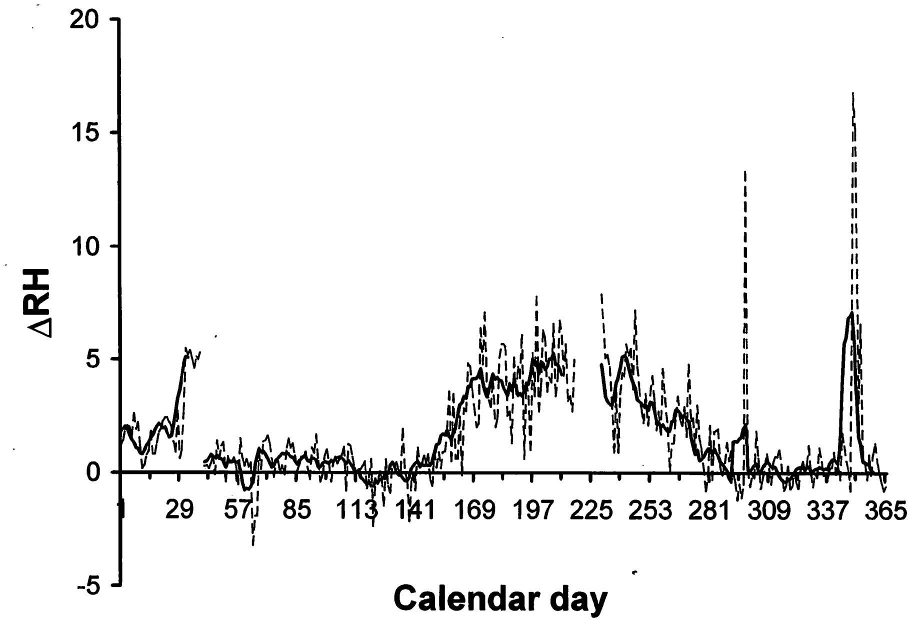

Fig. 4. Schematic diagram showing the model domain configuration. The variables *T*, *p*, and *q* indicate temperature, pressure, and water vapor mixing ratio, respectively. The model comprises NZ layers of thickness Δz, with canopy top at height z_c. The temperature T_{sky} determines the upper boundary condition, as described in the text.

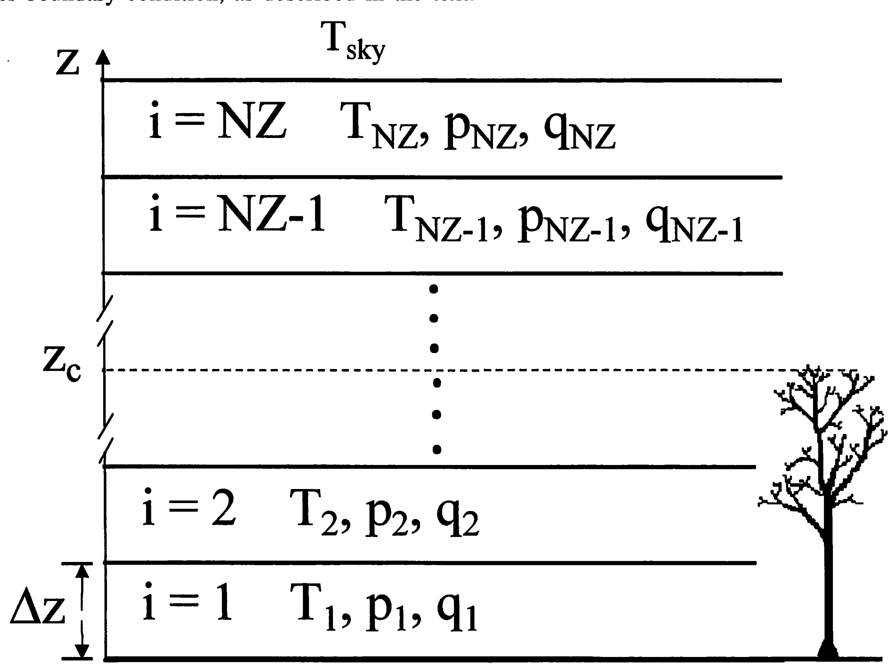

We used a vertical resolution of $\Delta z = 0.5$ m for the lower 30 m of the domain in our simulations. Above 30 m, each level was stretched by a factor of 1.053 compared with the next lower level. With 100 levels total, this yielded a domain 98.5 m deep with the top two levels 3.9 m apart. Because we made no atmospheric pressure measurements at the study site, we assumed surface pressure to be 100 kPa for the simulations, and the model computed pressure at each higher level hydrostatically. The ideal gas law, in conjunction with calculated temperature and pressure, determines the density of air at each level. We specified a time step of 60 s for the model integration.

The IRTM determines a downward radiative flux at the top of the domain from a user-specified effective sky temperature, T_{sky}. This temperature is used to compute a blackbody radiative flux according to the Stefan–Boltzmann law, and that flux is consequently used in the model for the downward flux into the domain. The value of T_{sky} depends on the properties of the atmosphere above the model domain and is, therefore, specific to each day, but not site, we examined. We used the previously mentioned radiosonde profiles for the atmosphere between the ground and the tropopause, along with the IRTM, to determine the downward flux at 100 m for GB and IF and converted these fluxes to effective blackbody

Table 3. Sky temperature (T_{sky}), optimum soil heat capacity (c_s*), and mean absolute error (MAE) associated with c_s* for each simulated night.

Night	T_{sky} (K)	c_s* (J·K^{-1}·m^{-2})	MAE (K)
100	249.2	0.4×10^5	2.37
152	256.9	0.3×10^5	1.97
304	246.9	0.8×10^5	0.48
313	246.2	0.7×10^5	0.7
103	247.0	0.8×10^5	1.81
125	255.0	0.6×10^5	1.1
137	255.4	0.6×10^5	2.04

temperatures. Assuming T_{sky} varies linearly between the two locations and that Park Falls, Wis., is on a line between the two sounding sites, we interpolated the temperatures to obtain a value for each day. The value of T_{sky} for each day was the same for the clear-cut, half-cut, and uncut sites.

The lower boundary of the model is at the ground surface, which is assumed to be a perfect blackbody radiator. The ground temperature at the start of the simulation is determined for each day by linear extrapolation of the observed temperatures at 0.25 and 0.5 m. While specification of ground temperature is straightforward, determination of a heat capacity for this lowest model layer is more complex. The thermal properties of soil can be readily measured, but when soil is covered by a complex mixture of leaf litter, dead woody matter, and herbaceous plants, the heat capacity of the combined materials is less obvious. Furthermore, the total upwelling radiation from this mixture depends on the contributions of all components, which may have different temperatures at different times because of differential cooling rates.

We used the model with the previously determined values of T_{sky} and the observed data from the clearcut to estimate a single value for soil heat capacity, c_s, for use in the model. To do this, we found the value of c_s for each clearcut night that minimized the mean absolute error (MAE) of the model simulation temperatures at 0.5 m above the ground. We calculate mean absolute error according to the formula:

$$[1] \qquad \mathrm{MAE} = \frac{1}{n_f} \sum_{n=1}^{n_f} | T_{sn} - T_{on} |$$

where n_f is the number of hours simulated for a given night, T_{sn} is the simulation temperature at 0.5 m at hour n, and T_{sn} is the observed temperature at 0.5 m at hour n. Table 3 shows the sky temperatures and optimum soil heat capacities for the nights considered. We averaged these optimum values for all seven nights and used the average value, 6 × 10^4 J·K^{-1}·m^{-2}, for all subsequent simulations.

To initialize the model, we used a combination of the research-site observations and the radiosonde data. We examined water vapor mixing ratios (kilograms of water per kilogram of air) in the GB and IF soundings. The sounding wherein the mixing ratio at the lowest sounding level above 10 m was closest to that measured at 10 m at the research site was used to extend the surface data upwards. The model then interpolated mixing ratios and temperatures from this extended profile to the individual model levels.

It was our intention to include only those physical processes necessary, with as few parameterized processes as possible. We did not include any dynamic or thermodynamic processes that would be negligible on radiative freeze-prone nights. We also did not include any representation of moisture flux to or from the ground or vegetation. Such a flux could take the form of transpiration, evaporation, or condensation (dew or frost formation). While this is assuredly unrealistic, it is necessary since accurate soil moisture and dew measurements are not available for the sites for the days and hours examined.

Biomass representation

The model uses the density of air and specific heat to compute temperature change for each layer. The specific heat of each layer below the forest canopy top reflects the contribution of biomass to the nocturnal forest energy budget. The layer-average specific heat including both air and biomass is

$$[2] \qquad c_f = c_a + \left(\frac{\rho_w c_w}{\rho_a} - c_a \right) \frac{A}{10^4}$$

where c_f is the average specific heat of the layer (J·kg^{-1}·K^{-1}), c_a is the specific heat of air at constant pressure (J·kg^{-1}·K^{-1}), ρ_a is the density of the air (kg·m^{-3}), ρ_w is the density of woody material (kg·m^{-3}), and c_w is the specific heat of woody material (J·kg^{-1}·K^{-1}). A is the horizontal cross-sectional area of radiatively active woody biomass (m^2·ha^{-1}). A real tree cools more on the surface than in the interior over a night. In the IRTM, all mass in a layer cools by the same amount. Essentially, the IRTM redistributes the energy loss experienced by a real tree so that all energy loss occurs in an isothermal layer of some thickness on the outside of the tree. This hypothetical outer layer cools by the same amount as the atmosphere and should yield an energy change equal to that the whole tree experiences in reality. We shall call the horizontal cross-sectional area of this outer layer, which has a thickness yet to be determined, the effective radiating area (ERA) of the tree or, by extension, a site.

We used a numerical model of heat conduction in a cylinder to determine the thickness of the ERA in a tree. This model assumes a cylinder of uniform density, thermal diffusivity, and initial temperature. It also assumes that temperature depends only on time and distance from the center of the cylinder. The model divides the cylinder, with radius a, into N incremental rings of width Δr. It uses a centered, leapfrog differencing scheme to compute heat conduction and subsequent temperature changes in the cylinder while the surface undergoes a sinusoidal forcing with a period of 24 h. We used the model to simulate a 12-h period, starting at the time of maximum temperature and continuing to the time of minimum temperature. The thermal diffusivity for these simulations was 1.5 × 10^{-7} m^2·s^{-1} (TenWolde et al. 1988). At the end of the 12-h period, the total energy change within the cylinder is

$$[3] \qquad \Delta E_c = 2\pi\rho c(\Delta r^2) \sum_{i=1}^{N} \Delta T_i\,(i - 0.5)$$

where ρ is the cylinder density, c is the specific heat of the cylinder, and ΔT_i is the temperature change experienced by the ith radial increment over the simulation.

The energy change for an isothermal outer layer on the cylinder would be

$$[4] \qquad \Delta E_i = 2\pi\rho c\delta a \Delta T_N$$

where δ is the thickness of the previously mentioned effective radiating layer. Setting eqs. 3 and 4 equal and solving for δ, we find

$$[5] \qquad \delta = \frac{\Delta r^2}{a\Delta T_N} \sum_{i=1}^{N} \Delta T_i(i - 0.5)$$

The results of the cylinder simulations showed that δ depends on cylinder radius, a, as shown in Fig. 5, but is independent of the amplitude of the forcing or the absolute value of the starting temperature. Using Fig. 5 and site survey data on tree diameters, we computed ERAs for the forest sites. The ERA for the halfcut site is 8.8 m^2·ha^{-2}, and ERA for the uncut site is 16.5 m^2·ha^{-2}.

Fig. 5. Relationship between thickness of effective radiating layer on a cylinder, δ, and cylinder radius, *a*.

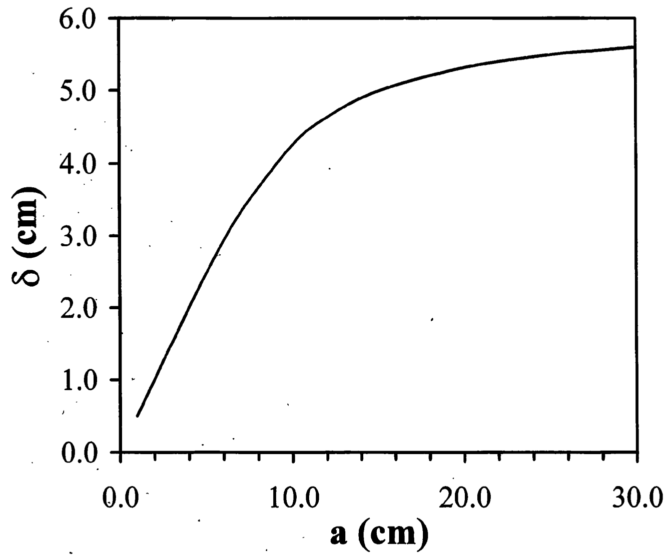

The value of c_a is constant at 1004 J·kg^{-1}·K^{-1}, while all other terms in eq. 2 are variable. For the present simulations, ρ_a is approximately 1.1 kg m^{-3}. Using ρ_w = 600 kg·m^{-3} and c_w = 2000 J·kg^{-1}·K^{-1} from TenWolde et al. (1988), the same values that we cited in the introduction, eq. 2 becomes

$$[6] \quad c_f = 1004 + 109A$$

Using the ERA values for the forest sites from above, the near-ground specific heat we computed for the model for the half-cut site is 1970 J·kg^{-1}·K^{-1} and that for the uncut site is 2800 J·kg^{-1}·K^{-1}. Based on the findings of Cannell (1984), we assumed that biomass volume (and hence ERA) decreased linearly from the ground upwards, to a value of zero at the canopy top, z_c. For these simulations, we set z_c at 20 m.

This model is admittedly and intentionally simplistic. There are also a number of assumptions involved, and we wish to state these explicitly so that the reader may understand the weaknesses of the model and perhaps recognize some other assumptions that were made unintentionally or implicitly. We ask the reader to bear in mind that this study represents an initial attempt to parameterize vegetation within the IRTM, and it is not expected or intended to be perfect or physically complete.

First and foremost of the assumptions made, we have ignored all sources of temperature change other than radiation and water phase changes. In short, we omitted sensible and latent heat fluxes across the top and bottom boundaries of the forest–atmosphere layer. Writing the thermodynamic equation for the forest layer as

$$[7] \quad \rho C \frac{\partial T}{\partial z} = \frac{\partial F_{\text{net}}}{\partial z} + H_v + Q$$

where ρ is density, *C* is heat capacity, *T* is temperature, F_{net} is the net radiative flux (positive upward), H_v is the energy absorbed or released by evaporation or condensation, we can combine the sensible and latent heat fluxes across the upper and lower boundaries of this layer into the term *Q*. The contributions to *Q* at the upper boundary are net heat fluxes, i.e., they include vertical gradients in them already. For fluxes at the upper boundary, vertical derivatives (as in $\partial(wT)/\partial z$ where *w* is vertical velocity) are contained in *Q*.

On nights when an inversion layer forms and the boundary layer is stable, ground fluxes will be directed from the air toward the colder ground; these constitute a negative contribution to *Q*. Sensible and latent heat fluxes at the leafless canopy top will be smaller in magnitude, again directed downward (Stull 1997). The ground fluxes dominate, and *Q* will be negative.

The radiative fluxes in the model will compensate for the exclusion of the other processes to some extent. Any compensation will be partial, however, and model cooling rates will likely be less than the cooling rates actually observed. In the end, the omission or inclusion of the sensible and latent heat fluxes in the model may not matter. Our interest lies in a comparison of simulations with and without biomass heat capacity. Any effect of biomass heat capacity on *Q* will be indirect and small, and the effect of the omitted processes will largely cancel out in the aforementioned comparisons.

We assume that the air and the trees are in thermal equilibrium at all times, with equal temperatures. Whether this results from conductive or radiative energy transfer between the air and trees is not important for the present purposes nor does the model resolve it. It cannot involve latent heat transfer, however, or it would violate the moisture balance in the model.

As a simplification, we have neglected the difference in emissivity between the trees and the air. Including such a quantity would have altered the geometry and the entire nature of the problem, rendering the IRTM inappropriate.

We have also neglected the radiating surface area of the trees. In reality, the rate of energy exchange depends on the surface area of the trees that are radiating, something the basal area does not reflect. If a given basal area comprises many small trees, the surface area of those trees would be quite large and the volume of wood per unit surface area would be small. This would lead to different radiative fluxes and cooling rates than would the same basal area comprising only a few, larger trees. Again, inclusion of this aspect would have altered the geometry and rendered useless the current IRTM.

Table 4. Results of clear-cut simulations.

Night	MAE (K)	E_s (kJ·m^{-2})	E_a (kJ·m^{-2})
100	3.33	−186	−26
152	2.92	−93	−21
304	1.26	−58	−17
313	0.84	−99	−22
103	1.95	−75	−20
125	1.10	−90	−24
137	2.04	−103	−23
Mean	1.92	−100	−22

Note: MAE is the mean absolute error of the simulations measured at the 0.5 m level E_s is the energy change in the model soil layer per hour of simulation, and E_a is the energy change in the lowest 20 m of the model atmosphere per hour of simulation.

Application

We used the IRTM to simulate the chosen nights in the clear-cut site. For each night, we noted the MAE measured at 0.5 m above the ground, the change in energy in the soil layer, and the change in energy of the lower 20 m of the atmosphere.

With the half-cut and uncut sites, we ran the model twice for each night. One run used the specific heat of air at all model levels (i.e., no biomass), and the other run had increased specific heat as described above (biomass runs). We recorded the same quantities for these simulations that we had recorded for the clear-cut runs.

The clear-cut simulations provide a measure of the model's accuracy in a situation fairly close to that it was originally designed to represent. The differences between observations and simulation here are largely due to nonradiative processes in reality, the fact the clearcut actually has vegetation in it, and the errors intrinsic in the model such as a crude soil representation and the

Table 5. Results of forested-site simulations without biomass.

	Half-cut			Uncut		
Night	MAE (K)	E_s (kJ·m^{-2})	E_a (kJ·m^{-2})	MAE (K)	E_s (kJ·m^{-2})	E_a (kJ·m^{-2})
100	2.53	–171	–27	2.02	–166	–22
152	2.28	–108	–20	3.04	–103	–21
304	2.79	–47	–19	2.94	–58	–18
313	4.47	–54	–27	2.74	–84	–24
103	2.49	–64	–21	3.22	–67	–21
125	1.06	–85	–25	1.52	–96	–23
137	1.75	–103	–22	2.04	–109	–22
Mean	2.48	–90	–23	2.50	–98	–22

Note: MAE is the mean absolute error of the simulations measured at the 0.5 m level, E_s is the energy change in the model soil layer per hour of simulation, and E_a is the energy change in the lowest 20 m of the model atmosphere per hour of simulation.

Table 6. Results of forested-site simulations with biomass.

	Half-cut			Uncut		
Night	MAE (K)	E_s (kJ·m^{-2})	E_a (kJ·m^{-2})	MAE (K)	E_s (kJ·m^{-2})	E_a (kJ·m^{-2})
100	2.92	–154	–35	2.08	–147	–32
152	1.60	–106	–25	1.61	–100	–29
304	1.87	–46	–22	1.31	–56	–24
313	2.94	-51	–32	0.97	–80	–31
103	2.12	–63	–24	2.27	–66	–26
125	0.97	–83	–31	0.90	–93	–32
137	1.4	–100	–28	1.21	–105	–30
Mean	1.97	–86	–28	1.48	–92	–29

Note: MAE is the mean absolute error of the simulations measured at the 0.5 m level, E_s is the energy change in the model soil layer per hour of simulation, and E_a is the energy change in the lowest 20 m of the model atmosphere per hour of simulation.

parameterized atmospheric optics. The MAE of the clear-cut simulations serves as a benchmark against which we compare the forest-site results.

Results and discussion

Clear-cut simulations

Table 4 shows the results of the clearcut simulations. The MAE, 1.92 K, is comparable with the MAE values listed by Figuerola and Mazzeo (1997) for models designed to predict nocturnal or dawn surface temperatures under calm, clear skies. The values of MAE these authors list range from 0.8 K for their own model to 4.4 K for the model of Brunt (1941), with an average model MAE of 2.6 K. These models are developed and used for prediction of radiative freezes in agricultural situations, where biomass heat storage is considered negligible.

As noted previously, there are several known sources of error in the model. While we made every effort to select nights dominated by radiative processes, there are inevitably some nonradiative processes occurring. The effect of these processes on the results varies by night. The clearcut is not a vacant field of short grass but has fairly dense cover of aspen in some areas. This alters the heat balance and is not something we tried to include in the model. The upper and lower boundary conditions used for the model also contribute to error. Even when we used the optimum soil heat capacity for each individual night, the average MAE was 1.50 K. Finally, there is error due to the model's parameterization of emissivities. Liou et al. (1984) found the model error near the ground to be on the order of 0.2°C per day, which would mean less than 0.1°C over the present 10-h simulations.

Forest site simulations

The results of the forest site simulations without biomass represented appear in Table 5. The MAE increases over the MAE for the clearcut simulations, by approximately 0.6 K. Energy losses are comparable with those seen in the clearcut simulations.

Table 6 shows the results of the forest site simulations with biomass included. Compared with the simulations without biomass, the MAE values have decreased for both the half-cut and uncut sites. Analysis of variance (ANOVA) comparing the half-cut MAE values with and without biomass shows no significant ($\alpha = 0.05$) difference between the two samples, but the same test for the uncut site simulations indicates a significant difference between the two samples. Energy losses for air and soil combined are slightly higher than in the simulations without biomass but not enough to be considered statistically distinct (based again on ANOVA with $\alpha = 0.05$)

For most days tested, MAE dropped when we added biomass. The reverse is true for day 100 at the uncut site. On this day, MAE increased when we included biomass.

We also examined the model bias with and without biomass, an indication of systematic differences between the model and observations. Model bias is the average difference between model and observed temperatures each hour at 0.5, 1.0, 2.5, and 10.0 m. For the half-cut site, adding biomass raised the model bias from –1.13 to 0.37°C. Including biomass in the uncut site simulations raised model bias from –1.15 to 1.06°C. Thus, for both sites, the no-biomass runs were too cold, and the biomass runs were too warm. Model bias at 0.5 m alone was less than model bias for all four heights combined, indicating that the model created an excessively strong inversion. If the model included any allowance for turbulence, the weak mixing one might expect on these calm nights (especially just after sunset) would weaken the inversion, thus bringing the model results closer to observed temperatures.

Conclusions

The model reproduced temperatures in the clearcut fairly well. Its performance was comparable with that of models used to predict radiative freezing in agricultural settings. In the forest-site simulations, the model results suggest that inclusion of biomass heat storage reduces model error. Nonetheless, including biomass leads to underestimation of cooling rates.

The results, at the least, support further examination of the role of forest biomass in the occurrence or absence of middle or late spring freezes. If such examination yields results that forest managers can use to reduce freeze damage to desired species, it can be of economic and ecological benefit. There are a number of refinements that can be made in the model, and there are field experiments that could serve to improve understanding of the magnitude of biomass heat storage.

The most significant improvement to the present model would be inclusion of turbulent fluxes in the atmosphere. Such an addition is not trivial, however, as it requires parameterization of turbulent eddies, which in turn depend on measured wind speeds. Since all of the nights used in this study had wind speeds below the instrument threshold for most of each night, the uncertainty in any parameterization could be large.

The model could be made more realistic in its treatment of water condensation. In a clearcut, excess water in the air will probably condense into fog, as in the present model. In a forest, much or all condensation would take the form of dew. Dew, unlike fog, has no impact on the opacity of air layers, and making forest moisture turn to dew would remove the increased absorption and emission that fog creates. A truly accurate model would need a more elaborate representation of vegetation and soil surface temperatures, separate from air temperatures; this may be useful in the future but is probably secondary in importance to other considerations.

An alternative to modifying the present model would be taking a completely different boundary layer model that already includes radiation, turbulence, and other heat fluxes, and altering the specific heat that model uses for subcanopy layers. Does including biomass in heat capacity have a significant effect on model results?

To better answer the question of how biomass heat storage influences freeze events, there are field measurements that would be of use. Improved knowledge of forest biomass profiles would be beneficial. These profiles would presumably show differences between partially open sites, with significant undergrowth, and closed canopy sites where shrub and suppressed tree volume are not as great.

This study depended on meteorological measurements taken at a small number of heights. A study designed specifically to collect data for freeze simulations, or nocturnal temperature evolution in general, using regularly spaced sensors of higher precision would allow a much stronger test of the model. On-site cloud, precipitation, and above-canopy downward radiation measurements would improve the reliability of the process for selecting "radiative freezelike" nights.

Other useful measurements would be the skin temperature of the ground and soil moisture content. Both of these would allow more accurate specification of the model's lower boundary condition.

Soil properties may also be important in addressing the broader question of how stand density (biomass) influences near-surface temperatures and thereby inhibits or encourages freezing. As the density of trees varies, so does the density of undergrowth, as well as the temperature and humidity regime near the ground. All of these factors influence soil composition and moisture content. Since composition and moisture both have an effect on soil heat capacity, these properties could be as important or more important than biomass heat storage in controlling near-ground temperatures.

Forest edge is more susceptible than forest interior to radiative freezing. This raises the question of what is the appropriate radius around a point for the measurement of the basal area or ERA at that point. Whether it is 5, 10, 20, or 100 m would significantly impact the model's accuracy for points near a forest edge. A field experiment monitoring the microclimate along a field-to-forest gradient could help answer this question, and allow extension of these results to forest gaps.

Acknowledgments

The authors thank Ron Teclaw of the North Central Research Station in Rhinelander, Wis., for his extensive work on the installation and maintenance of the instruments at the Willow Springs site and his assistance with the data. We also thank Dr. John Norman for his comments and suggestions regarding the conceptualization of biomass in the model; they greatly improved the model results. The comments of two anonymous reviewers were helpful in strengthening the presentation and several parts of the discussion. Finally, thanks go to Heidi Cherry for her comments and suggestions on an early draft of this paper.

References

Anderson, J.B., and Brower, L.P. 1996. Freeze-protection of overwintering monarch butterflies in Mexico: critical role of the forest as a blanket and an umbrella. Ecol. Entomol. **21**: 107–116.

Arya, S.P. 1988. Introduction to micrometeorology. Academic Press, San Diego, Calif.

Aussenac, G. 1970. Gelées tardives et jeunes peuplements forestiers. Rev. For. Fr. **22**(4): 463–469.

Baumgartner, A. 1956. Untersuchungen über den Wärme- und Wasserhaushalt eines jungen Waldes. Ber. Dtsch. Wetterdienstes No. 5(28).

Brunt, D. 1941. Physical and dynamical meteorology. 2nd ed. Cambridge University Press, New York.

Cannell, M.G.R. 1984. Woody biomass of forest stands. For. Ecol. Manage. **8**: 299–312.

Figuerola, P.J., and Mazzeo, N.A. 1997. An analytical model for the prediction of nocturnal and dawn surface temperatures under calm, clear-sky conditions. Agric. Meteorol. **85**: 229–237.

Geiger, R. 1965. The climate near the ground. Harvard University Press, Cambridge, Mass.

Kittredge, J. 1948. Forest influences. McGraw-Hill, New York.

Liou, K.N., and Ou, S.C. 1983. Theory of equilibrium temperature in radiative-turbulent atmosphere. J. Atmos. Sci. **40**: 214–229.

Liou, K.N., Ou, S.C., Kinne, S., and Koenig, G. 1984. Radiation parameterization programs for use in general circulation models. U.S. Air Force Geophys. Lab. Sci. Rep. No. AFGL-TR-84-0217.

Meesters, A.G.C.A., and Vugts, H.F. 1996. Calculation of heat storage in stems. Agric. For. Meteorol. **78**: 181–202.

Munn, R.E. 1966. Descriptive micrometeorology. Academic Press, New York.

Percy, R.W., Ehleringer, J., Mooney, H.A., and Rundel, P.W. 1989. Plant physiological ecology: field methods and instrumentation. Chapman & Hall, London.

Ringer, D., and Stearns, F. 1972. Influence of forest openings on climate. Univ. Wis. Milw. Field Stn. Bull. **5**(2): 8–12.

Stephens, G. 1978. Radiation profiles in extended water clouds. III. Parameterization schemes. J. Atmos. Sci. **35**: 2123–2132.

Stull, R.B. 1997. An introduction to boundary layer meteorology. Kluwer Academic Publishers, Dordrecht, the Netherlands.

Teclaw, R.M., and J.G. Isebrands 1993. An artificial regeneration system for establishing northern red oak on dry–mesic sites in the Lake States. Ann. Sci. For. **50**: 543–552.

TenWolde, A., McNatt, J.D., and Krahn, L. 1988. Thermal properties of wood and wood panel products for use in buildings. U.S. Dep. Energy Rep. No. DOE/USDA-21697/1.